PHYSICAL REVIEW C **79**, 044902 (2009)

Hadronic observables from Au + Au collisions at $\sqrt{s_{NN}} = 200$ GeV and Pb + Pb collisions at $\sqrt{s_{NN}} = 5.5$ TeV from a simple kinematic model

T. J. Humanic*
Department of Physics, Ohio State University, Columbus, Ohio, USA

(Received 3 October 2008; published 9 April 2009)

A simple kinematic model based on superposition of $p+p$ collisions, relativistic geometry, and final-state hadronic rescattering is used to calculate various hadronic observables in $\sqrt{s_{NN}} = 200$ GeV Au + Au collisions and $\sqrt{s_{NN}} = 5.5$ TeV Pb + Pb collisions. The model calculations are compared with experimental results from several $\sqrt{s_{NN}} = 200$ GeV Au + Au collision studies. If a short hadronization time is assumed in the model, this model describes the trends of the observables from these experiments surprisingly well considering the model's simplicity. This also gives more credibility to the model predictions presented for $\sqrt{s_{NN}} = 5.5$ TeV Pb + Pb collisions.

DOI: 10.1103/PhysRevC.79.044902 PACS number(s): 25.75.Dw, 25.75.Gz, 25.40.Ep, 25.40.Ve

I. INTRODUCTION

The experiments at the BNL Relativistic Heavy Ion Collider (RHIC) have produced many interesting studies of hadronic observables from relativistic heavy-ion collisions over the past six years or so. The goal has been to use these observables to characterize the conditions of the early state of matter in heavy-ion collisions so as to be possible signatures of exotic states, such as quark matter [1–4]. Hadronic observables measured at RHIC can be placed into four general categories: spectra, elliptic flow, femtoscopy, and high p_T. Examples of observables in each category relevant to the present work are the following: "spectra" encompasses rapidity, transverse momentum, and transverse mass distributions [5–7]; "elliptic flow," characterized by the quantity V_2, includes V_2 vs η and V_2 vs p_T distributions [8–11]; "femtoscopy," also known as Hanbury-Brown–Twiss interferometry [12], includes two-pion correlation studies vs transverse momentum and azimuthal angle [13,14]; and "high p_T," which is targeted to be sensitive to jet effects, includes R_{AA} vs p_T and $dn/d\Delta\phi$ distributions [7,15]. Models that describe the early stages of the collision after the initial nuclei have passed through each other in terms of partonic degrees of freedom, for example, as a cascade or in terms of hydrodynamics, have been successful in describing the experimental systematics of some of these observables in some kinematic ranges, but no single model has thus far succeeded in making an adequate overall description of the systematics of all these observables in a wide kinematic range (for a comprehensive overview of comparisons of models with RHIC experiments, see Refs. [1–4] and references therein).

The goal of the present work is to see how far one can get in describing the experimental systematics of all the observables mentioned above in a wide kinematic range using a simple kinematic model with hadronic degrees of freedom. In essence, the model is, for each heavy-ion collision, a superposition of $p+p$ collisions in the geometry of the colliding nuclei with a proper time for hadronization determining the initial space-time position of each produced particle, followed by a Monte Carlo hadronic rescattering calculation. The $p+p$ collisions are generated by the PYTHIA code [16] at the beam energy of interest. Some of the advantages of using this scheme are clear:

(i) One has access to all of the particle types available in PYTHIA.
(ii) It is conceptually simple: $p+p$ superposition + simple geometry + hadronic rescattering.
(iii) It has few free parameters; even the hadronization proper time can be set by a Tevatron study (see below).
(iv) Jets are automatically included in the model since PYTHIA has jets and thus hadronic observables depending on jets can be studied.
(v) The model should be easily scalable via PYTHIA to higher energies such as will be found at the CERN Large Hadron Collider (LHC), thus giving the possibility of making predictions for heavy-ion collisions at those energies.

There is no *a priori* reason why such an approach should be successful, and in fact there are reasons to think it should be unsuccessful, the most serious one being that it is hard to imagine that hadronic degrees of freedom, rather than partonic degrees of freedom, can be valid soon after the nuclei have passed through each other due to the expected high energy density. This would require a very short hadronization time in these collisions. On this point, it is encouraging that a recent study of pion HBT in Tevatron collisions has shown that a similar model for $p+p$ collisions can explain the p_T and multiplicity dependences for the extracted radius parameters if a very short proper time for hadronization of 0.1 fm/c is assumed [17].

Previous studies using a model similar to this in which hadronic degrees of freedom were assumed in the early stage of the heavy-ion collision followed by hadronic rescattering have been shown to give qualitative agreement with experimental results for some observables [18–20]. Although similar, there are significant differences between those previous studies and the present one:

(i) In the old model, the initial kinematic state of the hadrons in the collision was parametrized as a thermal distribution in p_T and a Gaussian distribution in rapidity

---

*humanic@mps.ohio-state.edu

in which the temperature of the thermal distribution and width and midrapidity density of the rapidity distribution (as well as the rapidity densities of different particle species) were fixed by comparisons with experiment. In the present model, superposed PYTHIA $p + p$ collisions provide all the information about the initial kinematic state of the hadrons, including jets, which were not present in the old model.

(ii) In the old model, the initial hadronic geometry was taken to be similar to a "Bjorken tube," in that there was no initial expansion in the direction transverse to the beam direction, but initial expansion could occur along the longitudinal direction controlled by the hadronization proper time. In the present model, initial expansion is also allowed in the transverse direction to satisfy causality in this picture [see Eqs. (1) and (2) below].

(iii) In the previous studies, calculations were done at fixed impact parameter, so comparisons with experimental results that had been measured in centrality windows from multiplicity cuts were only qualitative. In the present study, the model is run in a "minimum bias" mode in which a distribution of impact parameters is calculated and comparisons with experiments are made using multiplicity cuts to obtain centrality windows equivalent to those from experiment, allowing quantitative comparisons with experiment.

(iv) In the previous studies, hadronic observables were only calculated for the "soft sector," i.e., $p_T < 2$ GeV/c, because p_T distributions for hadrons from the old model became exponentially larger than experiment for $p_T >$ 2–3 GeV/c. It has been found that this behavior was due to an error in the inelastic scattering algorithm in the old model and has been corrected in the present model. Thus, "hard sector," i.e., $p_T > 2$ GeV/c, studies are now possible.

Still, the only way to determine whether such a radical and simple picture for heavy-ion collisions is valid at all is to compare the results of the model with a range of experimental data. Being such a simple model, the main hope will be to give, at best, a qualitative description of the trends of the experimental hadronic observables mentioned above. This would already be a useful result, since it would help establish the hadronization time scale in RHIC heavy-ion collisions.

To this end, model calculations will be compared with results from the RHIC experiments PHOBOS [5,8], STAR [6,9,10,13–15], and PHENIX [7,11] for Au + Au collisions at $\sqrt{s_{NN}} = 200$ GeV. The goal will be to make comparisons as quantitative as possible between model and experiments. Predictions from the model for LHC-energy Pb + Pb collisions at $\sqrt{s_{NN}} = 5.5$ TeV will also be given.

The paper is organized into the following sections. Section II gives a description of the model, Sec. III presents results of the model for Au + Au collisions at $\sqrt{s_{NN}} = 200$ GeV and comparisons with RHIC experiments, Sec. IV presents predictions from the model for $\sqrt{s_{NN}} = 5.5$ TeV Pb + Pb collisions, and Sec. V gives a summary and conclusions.

II. DESCRIPTION OF THE MODEL

The model calculations are carried out in five main steps: (A) generate hadrons in $p + p$ collisions from PYTHIA, (B) superpose $p + p$ collisions in the geometry of the colliding nuclei, (C) employ a simple space-time geometry picture for the hadronization of the PYTHIA-generated hadrons, (D) calculate the effects of final-state rescattering among the hadrons, and (E) calculate the hadronic observables. These steps will now be discussed in more detail.

A. Generation of the $p + p$ collisions with PYTHIA

The $p + p$ collisions were modeled with the PYTHIA code [16], version 6.409. The parton distribution functions used were the same as used in Ref. [17]. Events were generated in "minimum bias" mode, i.e., setting the low-p_T cutoff for parton-parton collisions to zero [or in terms of the actual PYTHIA parameter, $ckin(3) = 0$] and excluding elastic and diffractive collisions (PYTHIA parameter $msel = 1$). Runs were made both with $\sqrt{s} = 200$ GeV and 5.5 TeV to simulate RHIC and LHC collisions, respectively. Information saved from a PYTHIA run for use in the next step of the procedure were the momenta and identities of the "direct" (i.e., redundancies removed) hadrons (all charge states) π, K, p, n, Λ, ρ, ω, η, η', ϕ, and K^*. These particles were chosen because they are the most common hadrons produced and thus should have the greatest effect on the hadronic observables in these calculations. Although Δs were included in the rescattering process (see below) during which they are produced abundantly, they were not input directly from PYTHIA since their lifetime is short, i.e., ≈1 fm, and thus their initial presence was judged to not effect the results significantly. Figure 1 shows an absolute comparison between

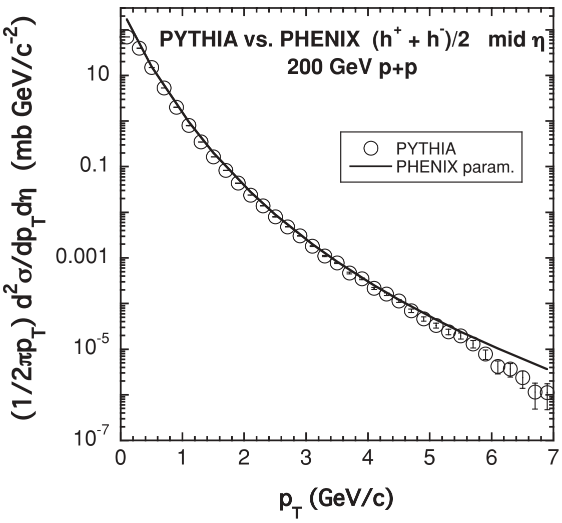

FIG. 1. $d\sigma/dp_T$ from PYTHIA compared with a PHENIX parametrization for 200 GeV $p + p$ collisions.

the invariant cross section distribution for charged particles from the PYTHIA $p + p$ run (with resonances decayed) used to generate the Au + Au collisions in the present model with a parametrization for 200 GeV $p + p$ collisions from PHENIX [7]. As seen, PYTHIA agrees quite well with the PHENIX parametrization up to about 6 GeV/c, showing that the $p + p$ collisions input into the model are quite reasonable.

B. Superposition of $p + p$ events to simulate heavy-ion collisions

An assumption of the model is that an adequate job of describing the heavy-ion collision can be obtained by superposing PYTHIA-generated $p + p$ collisions calculated at the beam $\sqrt{s}$ within the collision geometry of the colliding nuclei. Specifically, for a collision of impact parameter b, if $f(b)$ is the fraction of the overlap volume of the participating parts of the nuclei such that $f(b = 0) = 1$ and $f(b = 2R) = 0$, where $R = 1.2A^{1/3}$ and A is the mass number of the nuclei, then the number of $p + p$ collisions to be superposed will be $f(b)A$. The positions of the superposed $p + p$ pairs are randomly distributed in the overlap volume and then projected onto the x-y plane which is transverse to the beam axis defined in the z direction. The coordinates for a particular $p + p$ pair are defined as x_{pp}, y_{pp}, and $z_{pp} = 0$. The positions of the hadrons produced in one of these $p + p$ collisions are defined with respect to the position so obtained of the superposed $p + p$ collision (see below).

For fine tuning of the model so as to get slightly better agreement with the PHOBOS rapidity distributions [5], a lower multiplicity cut was made on the $p + p$ events used in the heavy-ion calculations. For $\sqrt{s_{NN}} = 200$ GeV Au + Au calculations, the cut was set to 20, which cut out approximately 26% of $p + p$ events; and for $\sqrt{s_{NN}} = 5.5$ TeV Pb + Pb calculations, the cut was set to 38 to cut out a similar fraction of $p + p$ events at that energy. It should be emphasized that this was indeed a "fine-tuning" cut—if it is not made, the overall results presented below from the model do not change appreciably, showing the robustness of the model calculations to this cut.

C. The space-time geometry picture for hadronization

The space-time geometry picture for hadronization from a superposed $p + p$ collision located at (x_{pp}, y_{pp}) consists of the emission of a PYTHIA particle from a thin uniform disk of radius 1 fm in the x-y plane followed by its hadronization, which occurs in the proper time of the particle, τ. The space-time coordinates at hadronization in the laboratory frame (x_h, y_h, z_h, t_h) for a particle with momentum coordinates (p_x, p_y, p_z), energy E, rest mass m_0, and transverse disk coordinates (x_0, y_0), which are chosen randomly on the disk, can then be written as

$$x_h = x_{pp} + x_0 + \tau \frac{p_x}{m_0}, \tag{1}$$

$$y_h = y_{pp} + y_0 + \tau \frac{p_y}{m_0}, \tag{2}$$

$$z_h = \tau \frac{p_z}{m_0}, \tag{3}$$

$$t_h = \tau \frac{E}{m_0}. \tag{4}$$

Equations (1) and (2) show the initial expansion in the transverse direction now present in the model. The simplicity of this geometric picture is now clear: it is just an expression of causality with the assumption that all particles hadronize with the same proper time τ. A similar hadronization picture (with an initial point source) has been applied to e^+-e^- collisions [21]. For all results presented in this work, τ will be set to 0.1 fm/c to be consistent with the results found in the Tevatron HBT study mentioned earlier [17].

D. Final-state hadronic rescattering

The hadronic rescattering calculational method used is similar to that employed in previous studies [18,19], except, as mentioned above, the error found in the algorithm to calculate inelastic scattering has been corrected. Rescattering is simulated with a semiclassical Monte Carlo calculation which assumes strong binary collisions between hadrons. Relativistic kinematics is used throughout. The hadrons considered in the calculation are the most common ones: pions, kaons, nucleons, and lambdas (π, K, N, and Λ), and the $\rho, \omega, \eta, \eta', \phi, \Delta$, and K^* resonances. For simplicity, the calculation is isospin averaged (e.g., no distinction is made among a π^+, π^0, and π^-).

The rescattering calculation finishes with the freeze-out and decay of all particles. Starting from the initial stage ($t = 0$ fm/c), the positions of all particles in each event are allowed to evolve in time in small time steps ($\Delta t = 0.5$ fm/c) according to their initial momenta. At each time step, each particle is checked to see (a) if it has hadronized [$t > t_h$, where t_h is given in Eq. (4)], (b) if it decays, and (c) if it is sufficiently close to another particle to scatter with it. Isospin-averaged s-wave and p-wave cross sections for meson scattering are obtained from Prakash *et al.* [22], and other cross sections are estimated from fits to hadron scattering data in Ref. [23]. Both elastic and inelastic collisions are included. The calculation is carried out to 200 fm/c for $\sqrt{s_{NN}} = 200$ GeV Au + Au collisions and to 400 fm/c for $\sqrt{s_{NN}} = 5.5$ TeV Pb + Pb collisions, which allows enough time for the rescattering to finish (as a test, calculations were also carried out for longer times with no changes in the results). Note that when this cutoff time is reached, all undecayed resonances are allowed to decay with their natural lifetimes, and their projected decay positions and times are recorded.

Figure 2 shows the time evolution plotted up to 50 fm/c of the particle density calculated at midrapidity, i.e., in the rapidity range $-1 < y < 1$, and the number of rescatterings per time step from the model for minimum bias (see below) $\sqrt{s_{NN}} = 200$ GeV Au + Au collisions. The solid lines show the average values of the quantities, whereas the dotted lines show the average $+\sigma$ to give an idea of the width of the distribution. The density is seen to start out high at 6–10 fm^{-3} and then to fall off rapidly with time such that by 4 fm/c the density is at or below 1 fm^{-3}. The rescattering rate starts small in the first time bin because of time dilation of the

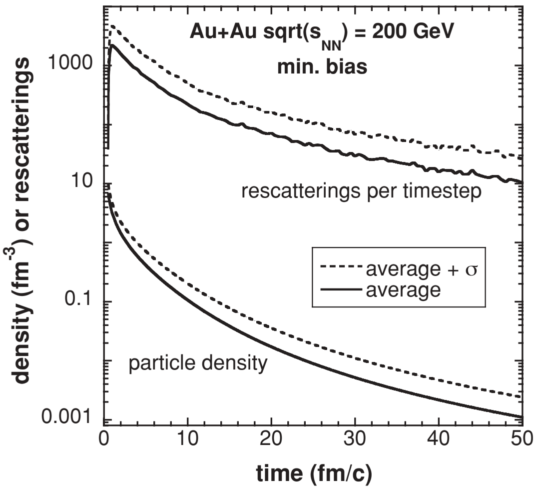

FIG. 2. Time evolution up to 50 fm/c of the particle density calculated at midrapidity ($-1 < y < 1$) and the number of rescatterings per time step from the model for minimum bias $\sqrt{s_{NN}} = 200$ GeV Au + Au collisions. The solid lines show the average values of the quantities; the dotted lines show the average $+\sigma$.

hadronization time and the requirement imposed in the model that particles must hadronize before they can scatter. By the second time step, the rescattering rate increases quickly and then falls off rapidly with time as does the density. The time evolution of the density will be discussed more later.

The rescattering calculation is described in more detail elsewhere [18,19]. The validity of the numerical methods used in the rescattering code have recently been studied using the subdivision method, the results of which have verified that the methods used are valid [20].

E. Calculation of the hadronic observables

Model runs are made to be "minimum bias" by having the impact parameters of collisions follow the distribution $d\sigma/db \propto b$, where $0 < b < 2R$. Observables are then calculated from the model in the appropriate centrality bin by making multiplicity cuts as done in the experiments, as well as kinematic cuts on rapidity and p_T. For the present study, a single 87 000-event minimum bias run was made from the model for $\sqrt{s_{NN}} = 200$ GeV Au + Au collisions which was then used to calculate all the hadronic observables from the model which are shown in this work for that system. In this way, a consistent picture of the agreement between the model and experiments can emerge, since it is virtually impossible to optimize the model to agree with experiment for a particular observable without spoiling the agreement for others which are calculated from the same run. In the case of the $\sqrt{s_{NN}} =$ 5.5 TeV Pb + Pb predictions, a single minimum bias run with 800 events was made.

III. RESULTS FROM THE MODEL FOR Au + Au COLLISIONS AT $\sqrt{s_{NN}} = 200$ GeV AND COMPARISONS WITH RHIC EXPERIMENTS

Various hadronic observables have been calculated from the 87 000 minimum bias run from the model mentioned above and are now compared with measurements from RHIC experiments. The observables and the experiments with which they will be compared are

(i) Spectra: $dn/d\eta$ (PHOBOS), dn/dp_T (PHENIX), dn/dm_T (STAR)
(ii) Elliptic flow: V_2 vs η (PHOBOS), V_2 vs p_T charged particles (STAR), V_2 vs p_T identified particles, and V_2/n_q vs p_T/n_q (PHENIX)
(iii) HBT: $\pi\pi$ vs ϕ and $\pi\pi$ vs k_T (STAR)
(iv) High p_T: R_{AA} vs p_T (PHENIX), $dn/d\Delta\phi$ vs $\Delta\phi$ (STAR)

In the spirit of making the comparisons as quantitative as possible between model and experiments, unless explicitly specified otherwise, absolute normalizations are used for the model observables in the plots shown.

A. Spectra

Figures 3–5 show model comparisons with PHOBOS [5], PHENIX [6], and STAR [7] for η, p_T, and m_T distributions, respectively. In Figs. 3 and 4, the centrality dependence of charged hadrons is also shown, and in Fig. 5 the particle species dependence is shown.

In Fig. 3, the centrality dependence of the rapidity distribution is followed fairly well by the model, although it is seen that the model shapes are slightly broader than experiment and the overall agreement near midrapidity is at the 10–15% level. Since the model is "isospin averaged," the model distributions are multiplied by 2/3 to approximate all charged particles.

In Fig. 4, the experimental centrality dependence is once again seen to be described reasonably well by the model, especially the absolute scale at low p_T. At higher p_T, particularly in the minimum bias case, the model underpredicts the absolute scale by as much as a factor of 4 at some points over the p_T range, yet still follows the trend of the data up to the highest p_T shown. To approximate $(h^+ + h^-)/2$ for the model, the model distributions are multiplied by 1/3.

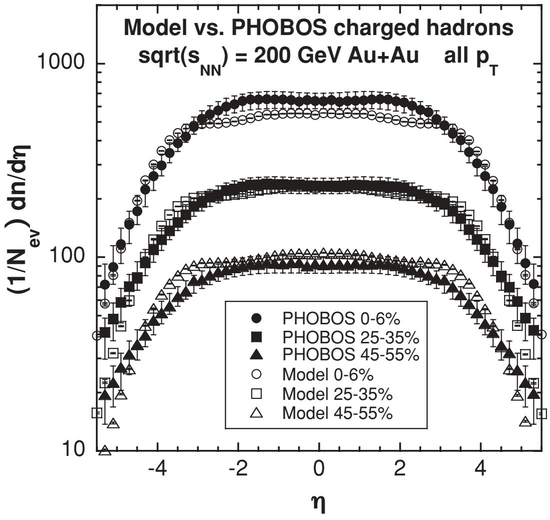

FIG. 3. Rapidity distributions for the model compared with PHOBOS for several centralities.

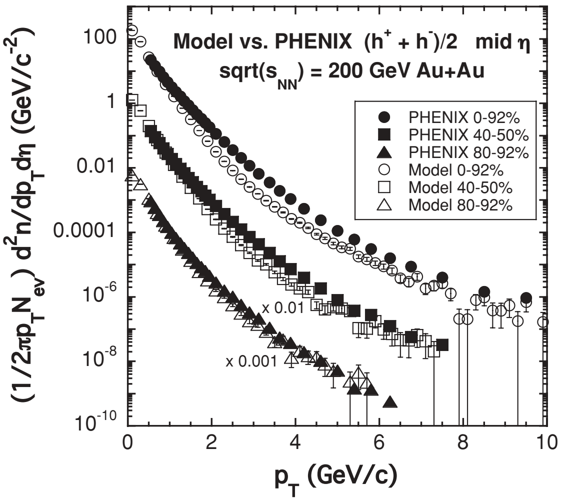

FIG. 4. p_T distribution for charged hadrons for the model compared with PHENIX for several centralities. The meaning of "mid-η" in this case is that the PHENIX spectra are measured in the range $-0.18 < \eta < 0.18$, whereas the model spectra are calculated in the range $-1 < \eta < 1$ for better statistics.

In Fig. 5, the absolute scale of the experimental particle species dependence is reproduced reasonably well by the model, as well as the "radial flow effect" of the slopes decreasing with increasing particle mass, but the absolute slopes from the model at low $m_T - m_0$ are seen to be uniformly somewhat too large (as is also seen in Fig. 4 at low p_T). The model distributions are multiplied by 1/3 to approximate positive charges.

Although there are clear differences seen in details between model and experiments as described above, it is still remarkable that this simple model does as well as it does in reproducing the overall absolute scales and dependences of these "bread and butter" experimental distributions. It is judged that the description by the model of these basic observables is adequate enough to cautiously proceed with using the model to calculate the derived observables such as elliptic flow, HBT, etc.

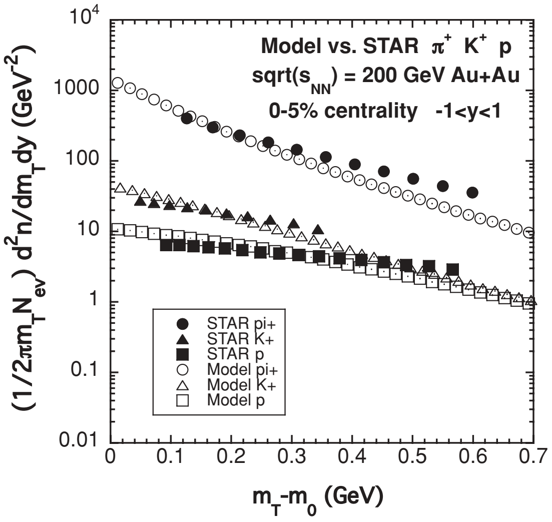

FIG. 5. m_T distributions for identified particles for the model compared with STAR.

B. Elliptic flow

The elliptic flow variable V_2 is defined as

$$V_2 = \langle \cos(2\phi) \rangle, \qquad \phi = \arctan\left(\frac{p_y}{p_x}\right), \tag{5}$$

where "⟨⟩" implies a sum over particles in an event and a sum over events, and where p_x and p_y are the x and y components of the particle momentum: x is in the impact parameter direction, i.e., reaction plane direction, and y is in the direction perpendicular to the reaction plane. The V_2 variable is calculated from the model using Eq. (5) and taking the reaction plane to be the model x-z plane.

Figures 6–11 show comparisons between the model and experiments for elliptic flow. Figure 6 compares the model to PHOBOS for charged particles for V_2 vs η in a centrality window of 25–50% [8]. The model is seen to agree with the measurements within error bars for the entire range in η, i.e., $-6 < \eta < 6$, although it looks systematically about 10% lower than experiment around midrapidity. Note that in the model, V_2 is completely determined by rescattering such that if the rescattering is turned off, $V_2 = 0$ in all kinematic regions.

Figure 7 shows a comparison of the model to V_2 vs p_T for $p_T < 2$ GeV/c for charged particles in several centrality bins from STAR [9]. The model is seen to do a reasonable job in representing the different centralities, although it is systematically higher than measurement by about 0.01–0.02 over the entire p_T range for the 0–5% centrality bin. Figure 8 compares the model with STAR for V_2 vs p_T for charged particles in a centrality bin 10–40% in a wide p_T range, i.e., $p_T < 6$ GeV/c [10]. What is remarkable about this

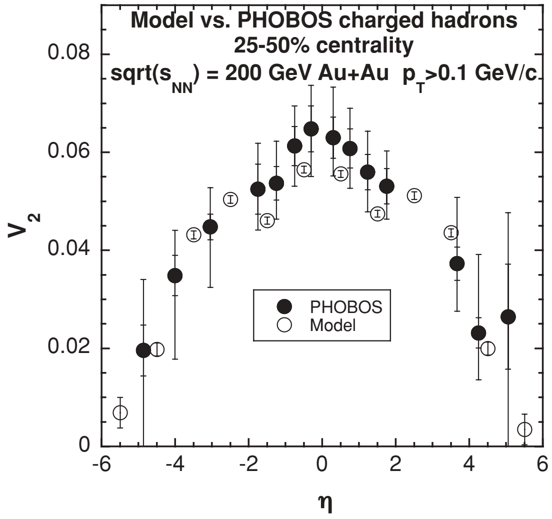

FIG. 6. V_2 vs η for the model compared with PHOBOS 25–50% centrality. The inner error bars on the PHOBOS data points show the statistical error, and the outer error bars show the statistical + systematic error.

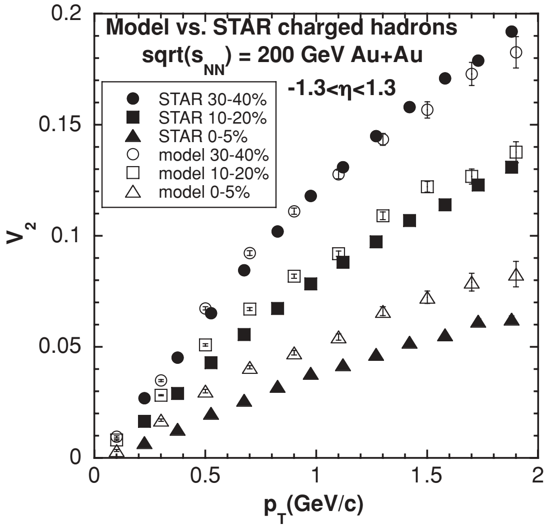

FIG. 7. V_2 vs p_T for the model compared with STAR for charged particles and several centralities.

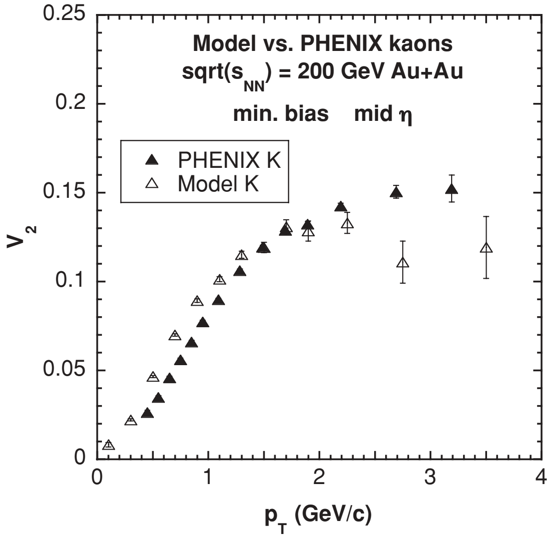

FIG. 9. V_2 vs p_T for the model vs PHENIX for kaons. The meaning of "mid-η" in this case is that the PHENIX spectra are measured in the range $-0.35 < \eta < 0.35$, whereas the model spectra are calculated in the range $-1.3 < \eta < 1.3$ for better statistics.

comparison is that the model describes the p_T behavior of the experiment in which V_2 increases for $p_T < 2$ GeV/c, flattens out, and then starts decreasing for $p_T > 3$ GeV/c. Once again, this behavior is completely rescattering-driven in the model.

In Figs. 9 and 10, the model is compared with identified-particle V_2 vs p_T plots for kaons, and pions and protons, respectively, and for minimum bias centrality from PHENIX [11]. For both figures, the low-p_T behavior, i.e., $p_T < 2$ GeV/c, is described well and quantitatively by the model, whereas the high-p_T behavior, i.e., $p_T > 2$ GeV/c, is only described qualitatively. In Fig. 9, the high-p_T behavior of the kaons flattens out for both experiment and model, but for the model it flattens out to a slightly lower value. In Fig. 10, the high-p_T behavior for the pions is to flatten out and start decreasing as the model also does but to a lower value, whereas the proton V_2 continues increasing, as it does for the model nucleons, but the model does not increase as fast (and the model 3.5 GeV/c point decreases).

Figure 11 shows the plots in Figs. 9 and 10 replotted in terms of the number of valence quarks in the identified particle, n_q, as V_2/n_q vs p_T/n_q. The point of doing this is to show that the different identified particles follow a universal curve when plotted on the same graph this way. Not surprisingly in the context of the discussion above, the model is seen to follow the experimental scaling quantitatively for $p_T/n_q < 1$ GeV/c and qualitatively at a lower value for $p_T/n_q > 1$ GeV/c.

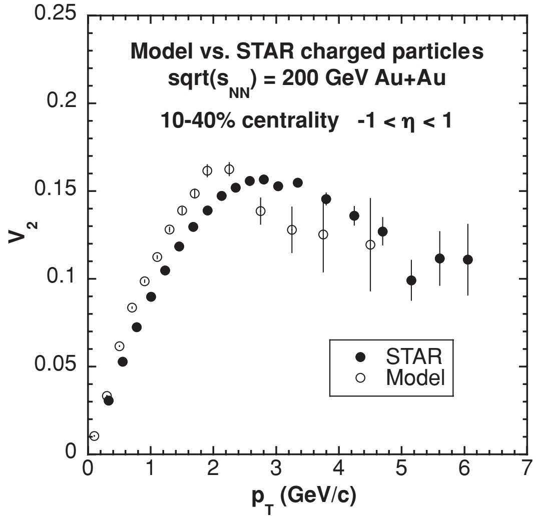

FIG. 8. V_2 vs p_T for the model vs STAR for charged particles and up to high p_T.

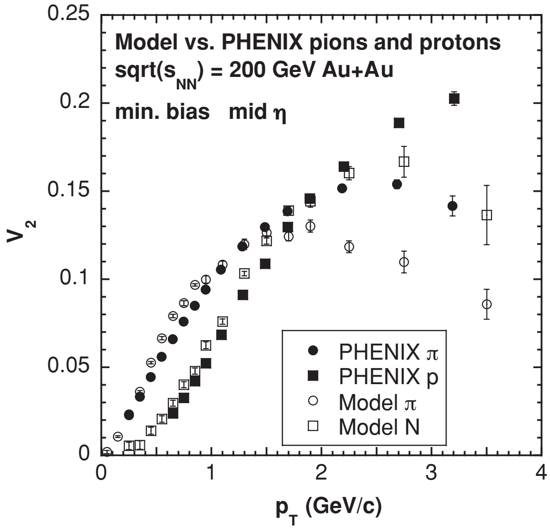

FIG. 10. Same as Fig. 9, but for pions and protons.

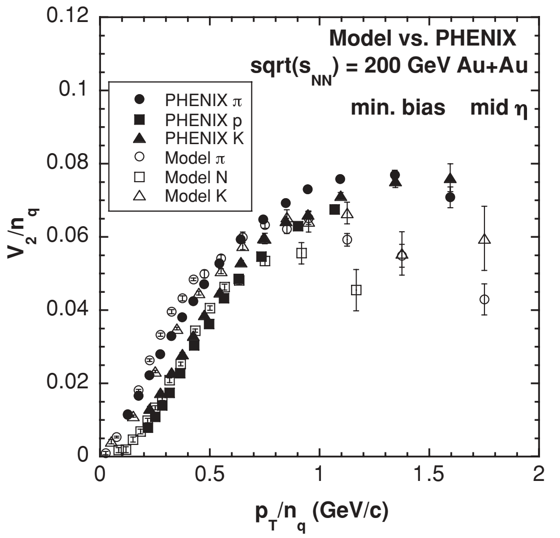

FIG. 11. V_2/n_q vs p_T/n_q for the model vs PHENIX for pions, kaons, and protons.

C. Two-pion femtoscopy (Hanbury-Brown–Twiss interferometry)

For the HBT calculations from the model, the three-dimensional two-pion correlation function is formed, and a Gaussian function in momentum difference variables is fitted to it to extract the pion source parameters. Boson statistics are introduced after the rescattering has finished (i.e., when all particles have "frozen out") using the standard method of pair-wise symmetrization of bosons in a plane-wave approximation [24]. The three-dimensional correlation function $C(Q_{\text{side}}, Q_{\text{out}}, Q_{\text{long}})$ is then calculated in terms of the momentum-difference variables Q_{side}, which points in the direction of the sum of the two pion momenta in the transverse plane; Q_{out}, which points perpendicular to Q_{side} in the transverse plane; and the longitudinal variable along the beam direction, Q_{long}.

The final step in the calculation is extracting fit parameters by fitting a Gaussian parametrization to the model-generated two-pion correlation function given by [25]

$$\begin{aligned} C(Q_{\text{side}}, Q_{\text{out}}, Q_{\text{long}}) &= G\big[1 + \lambda \exp\big(-Q_{\text{side}}^2 R_{\text{side}}^2 - Q_{\text{out}}^2 R_{\text{out}}^2 - Q_{\text{long}}^2 R_{\text{long}}^2 \\ &\quad - Q_{\text{out}} Q_{\text{side}} R_{\text{outside}}^2\big)\big], \end{aligned} \tag{6}$$

where the R parameters, called the radius parameters, are associated with each momentum-difference variable direction, G is a normalization constant, and λ is the usual empirical parameter added to help in the fitting of Eq. (6) to the actual correlation function ($\lambda = 1$ in the ideal case). The fit is carried out in the conventional LCMS frame (longitudinally comoving system) in which the longitudinal boson pair momentum vanishes [25]. Figure 12 shows a sample projected correlation function from the model with projected fit to Eq. (6).

Figures 13 and 14 show comparisons between the model and STAR for radius parameters extracted as a function of azimuthal angle ϕ, for two centrality cuts, 0–5% and 40–80%, respectively [13]. In Fig. 13, the model is seen to describe the more or less "flat" dependence on ϕ for R_{out}, R_{side}, and R_{long} seen in the experiment for these central collisions, although the model underpredicts the magnitude of R_{side} by about 20%. The model follows the trend of the experiment for R_{outside}^2 within the large statistical error bars shown. For the less central collisions shown in Fig. 14, the model describes the oscillatory behavior now seen in R_{out} and R_{side} as well as R_{outside}^2 and the continued flat dependence seen in R_{long}, although once again underpredicting the magnitude of R_{side} by about 30%. The λ parameters extracted in the fits from the model were constant in ϕ with the values 0.61 and 0.54 for the 0–5% and 40–80% centrality bins, respectively.

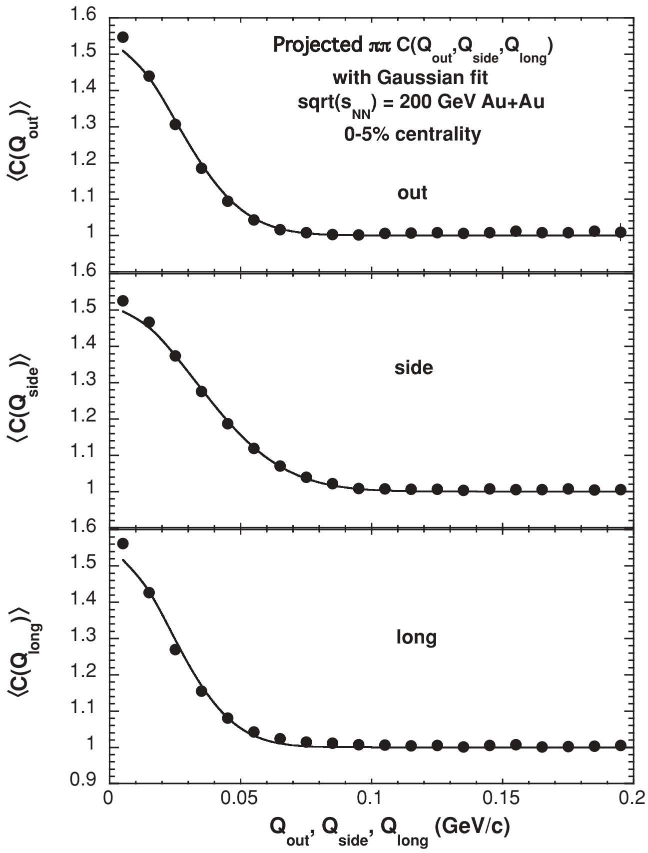

FIG. 12. Sample two-pion correlation function with Gaussian fit projected onto the Q_{out}, Q_{side}, and Q_{long} axes from the model. The collision centrality is 0–5% with cuts on the pions $-0.5 < y < 0.5$, $0.15 < p_T < 0.8$ GeV/c, and $0.15 < k_T < 0.25$ GeV/c.

Figure 15 compares the model with STAR for the k_T dependence of the radius parameters in a centrality bin of 0–5% [14]. For these fits, the parameter R_{outside} in Eq. (6) is set to zero. Several methods used by STAR in extracting their fit parameters were used, and as seen they give approximately the same basic results [14]. The model is seen to follow the general trend of the experiment for decreasing radius parameters for increasing k_T. The model slightly overpredicts this effect for R_{long} and, as was the case in the azimuthal HBT results shown earlier, consistently underpredicts the magnitude of R_{side} by about 24%. As seen in the experiment, the model λ parameter is less than unity, being constant in k_T at about 0.61, but larger than the experimental values on average by about 30%. Note

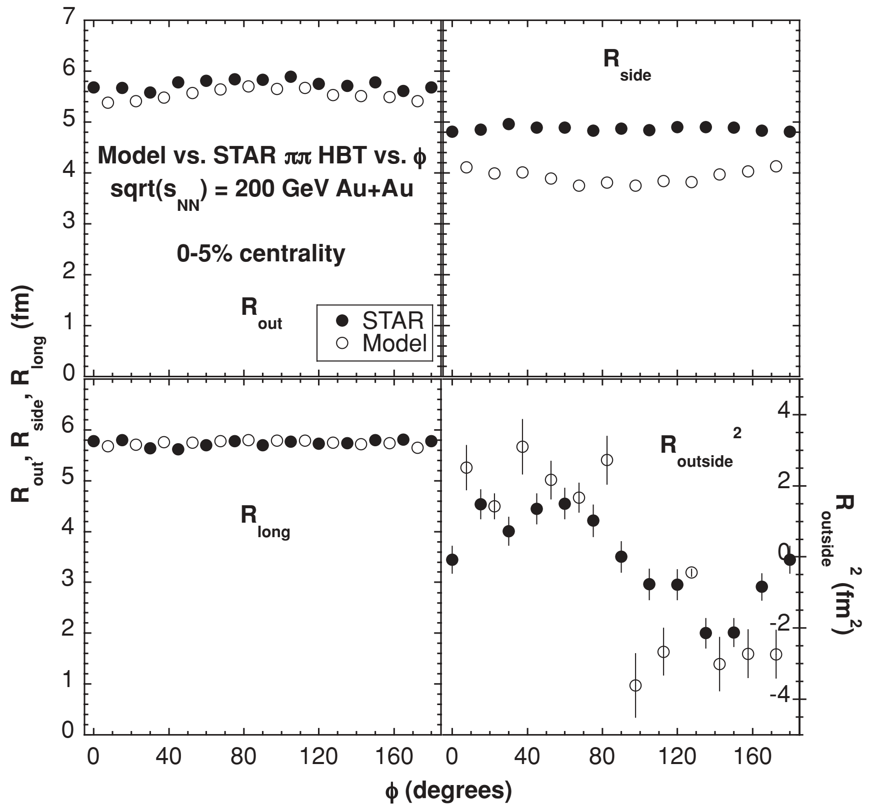

FIG. 13. Azimuthal two-pion HBT parameters vs ϕ from the model vs STAR for centrality 0–5%. Pions are accepted in the cut ranges $-1 < y < 1$, $0.1 < p_T < 0.6$ GeV/c, and $0.15 < k_T < 0.6$ GeV/c.

that the main source of $\lambda < 1$ in the model is from the presence of long-lived resonances such as η and η'.

D. High p_T

Studying the high-p_T behavior of the observables R_{AA} and $dn/d\Delta\phi$ is thought to be a way of more directly studying QCD processes, such as jets, in heavy-ion collisions. As mentioned earlier, since the present model is based on using PYTHIA which uses QCD processes in calculating $p + p$ collisions, the model should contain these effects and thus should be suitable for comparing with experiments that measure these observables.

The R_{AA} is defined as [7]

$$R_{AA} = \left(\frac{1}{N_{ev}} \frac{d^2 N^{\mathrm{AuAu}}}{dp_T\, d\eta}\right) \Big/ \left(T_{\mathrm{AuAu}} \frac{d^2\sigma^{pp}}{dp_T\, d\eta}\right), \qquad (7)$$

where the numerator is the usual Au + Au p_T distribution as shown in Fig. 4, and the denominator has the $p + p$ p_T distribution normalized to cross section as in Fig. 1 and multiplied by the quantity T_{AuAu}, the Glauber nuclear overlap function, which is different for each centrality cut.

Figure 16 compares the model with PHENIX for R_{AA} vs p_T for three centrality windows [7]. For both the model and PHENIX, the plots in Figs. 1 and 4 were used in Eq. (7) to calculate these R_{AA} plots along with the T_{AA} values shown in Table I of Ref. [7]. The error bars shown for the PHENIX plots are a sum of both statistical error and the overall scale uncertainty, and they mostly reflect the scale uncertainty. As seen, the model describes three main qualitative features of the experiment: (1) for large p_T, the R_{AA} decreases with increasing p_T, and as the centrality window goes from minimum bias (0–92%) to peripheral (80–92%), (2) the scale of R_{AA} increases and (3) the dependence of R_{AA} on p_T tends to flatten out. It is also seen that, even with the uncertainty in the PHENIX overall normalization, the model scale tends to be lower than experiment, and at low p_T the peaks in the plots for the model occurs at about 1.3 GeV/c, whereas the peaks occur at about 2.3 GeV/c for experiment. These differences of the model with experiment reflect the differences already seen in the p_T distributions in Fig. 4, but the qualitative similarities as discussed above are clearly present out to the highest p_T shown.

Figure 17 shows $dn/d\Delta\phi$ vs ϕ plots from the model and a comparison of one of them with STAR charged particles [15]. The model plots, which include all hadrons, are made using the same cuts on rapidity and p_T as used by STAR, namely, for individual particles $|\eta| < 0.7$ and $p_T > 2$ GeV/c, and for particle pairs, one of which is a "trigger particle," from which $\Delta\phi$ is formed, $|\Delta\eta| < 1.4$ and $p_T^{\mathrm{Trig}} > 4$ GeV/c. The lines are fits to the model points to guide the eye, and the model $dn/d\Delta\phi$ normalizations are in counts per bin. Figure 17(a) shows a plot from PYTHIA for 200 GeV $p + p$ as a reference. The forward and backward peaks from di-jet production are clearly seen at $\Delta\phi = 0$ and $\pm\pi$, respectively. Figure 17(b) compares the model to STAR minimum bias $\sqrt{s_{NN}} = 200$ GeV Au + Au collisions. The scale for the STAR plot is shown on the right-hand axis of the figure. As seen, the model describes the shape of the experiment well, both the width of the forward peak and the relative height of the backward peak with respect

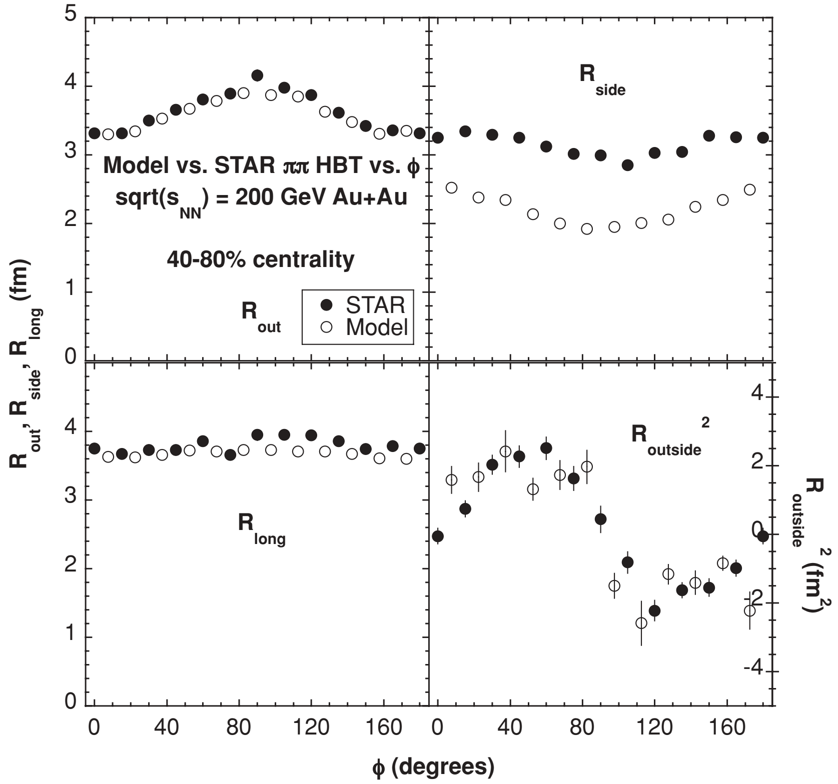

FIG. 14. Same as Fig. 13, but for centrality 40–80%.

to the height of the forward peak. Figure 17(c) shows a model plot for a medium centrality window at 10–30%. Features similar to the minimum bias plot are seen with a forward and backward peak of similar relative heights, although the width of the forward peak is somewhat larger than in the minimum bias case. A more central case from the model is shown in Fig. 17(d), where the centrality window is 0–10%. Although this plot is pushing the edge of the statistics possible from the 87 000-event model run used in this study for $\sqrt{s_{NN}} =$ 200 GeV Au + Au collisions, it appears to have a qualitatively different shape than the other plots shown in this figure. Namely, besides the presence of the forward peak, the plot looks more or less flat for values of $\Delta\phi$ out to $\pm\pi$, i.e., the backward peak appears suppressed. This is the same general behavior seen in STAR in the same centrality window, i.e., Fig. 1(c) of Ref. [15].

IV. PREDICTIONS FROM THE MODEL FOR Pb + Pb COLLISIONS AT $\sqrt{s_{NN}} = 5.5$ TeV

Predictions from the model for LHC-energy collisions for $\sqrt{s_{NN}} = 5.5$ TeV Pb + Pb collisions are presented below. These will be sample predictions for p_T and η distributions, elliptic flow, and HBT to give a flavor of the differences predicted by the model for LHC Pb + Pb collisions compared with RHIC Au + Au collisions. In this spirit, RHIC-energy Au + Au collisions with the same kinematic conditions as the LHC-energy Pb + Pb collisions will be shown to indicate the trends of the predictions. With the changes described above in Sec. II, the model will be used in the same way to make the $\sqrt{s_{NN}} = 5.5$ TeV Pb + Pb predictions as it was used for the $\sqrt{s_{NN}} = 200$ GeV Au + Au calculations, including the use of the short proper hadronization time of $\tau = 0.1$ fm/c.

Figures 18–21 show the model predictions for $\sqrt{s_{NN}} =$ 5.5 TeV Pb + Pb collisions compared with $\sqrt{s_{NN}} = 200$ GeV Au + Au collisions, also from the model. The most noticeable features of these predictions are summarized below:

(i) $dn/d\eta$ near midrapidity for charged particles is predicted to be about 1400 for a 0–5% centrality window at the LHC. This is seen in Fig. 18, which predicts that the midrapidity charged particle density for LHC Pb + Pb will be about a factor of 2.5 greater than for RHIC Au + Au. From Fig. 3 it was seen that the model density was about 10% lower than experiment. Thus even boosting the LHC prediction up by 10% puts its value at the lower end of the range of predictions which have been recently made of 1500–4000 in central collisions using various extrapolations of RHIC experimental rapidity densities [26].

(ii) The charged particle p_T distribution for $p_T > 5$ GeV/c is predicted to be about two orders of magnitude larger at the LHC than at RHIC. This is seen in Fig. 19 and is an expected consequence of the higher $\sqrt{s_{NN}}$ in the LHC collisions that the p_T distributions at high p_T should be greatly enhanced.

(iii) Elliptic flow in minimum bias centrality collisions is predicted to be slightly smaller at the LHC than at RHIC. As seen in Fig. 20, the plot of V_2 vs p_T for all hadrons for LHC Pb + Pb looks similar to that for RHIC Au + Au collisions, but overall the LHC plot

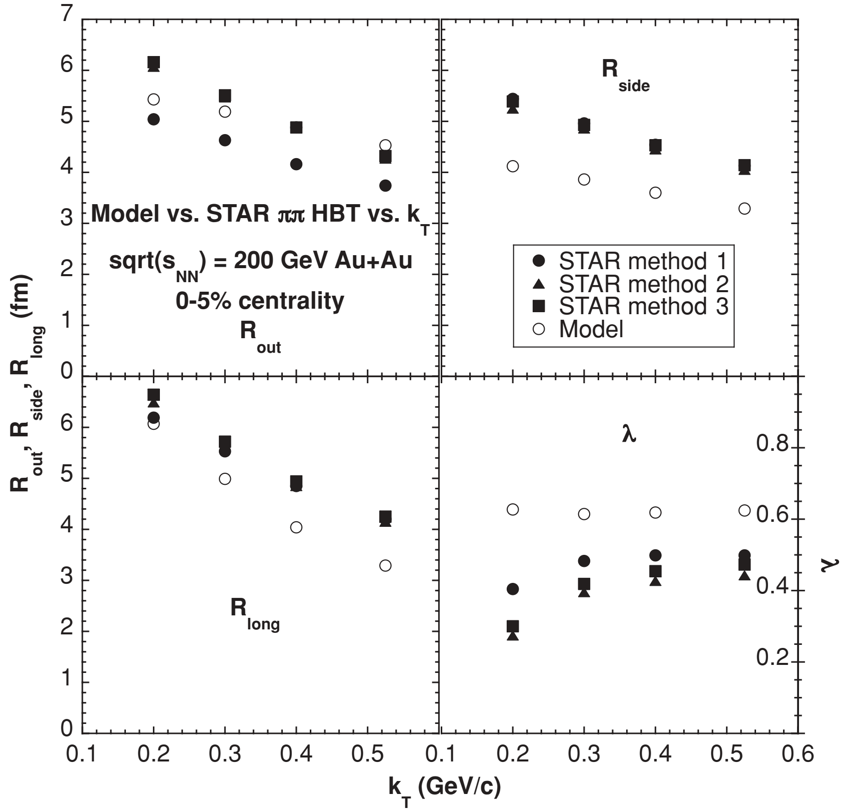

FIG. 15. Two-pion HBT parameters vs k_T from the model vs STAR for centrality 0–5%. Pions are accepted in the cut ranges $-0.5 < y < 0.5$ and $0.15 < p_T < 0.8$ GeV/c. The meaning of the three methods used by STAR to extract parameters may be found in Ref. [14]

gives a slightly smaller V_2 for the entire range in p_T. This is somewhat unexpected, since in this model V_2 is produced exclusively by the rescattering process, and since the rapidity density seen in Fig. 18 is higher at LHC, it might be expected that the more rescattering would result in a higher V_2 than for RHIC. Rather than this, it seems as though the initial "almond-shaped" geometry present in the $b > 0$ collisions starts to become "washed out" from the enhanced number of rescatterings. This will be discussed more below.

(iv) $\pi\pi$ HBT radius parameters in 0–5% centrality collisions are predicted to be 20–30% larger at the LHC than at RHIC. In Fig. 21, the behavior of the k_T dependence of the HBT parameters for LHC Pb + Pb is similar to what is seen for RHIC Au + Au, but the overall scale for the radius parameters is slightly larger.

V. DISCUSSION

Although some discussion of the individual results has been given above, it is useful to reflect on the sources of the effects in the present model that produce these results and to describe what interconnections may exist among them. Whereas PYTHIA provides the baseline $p + p$ kinematics, the hadronic rescattering is responsible for all collective effects in

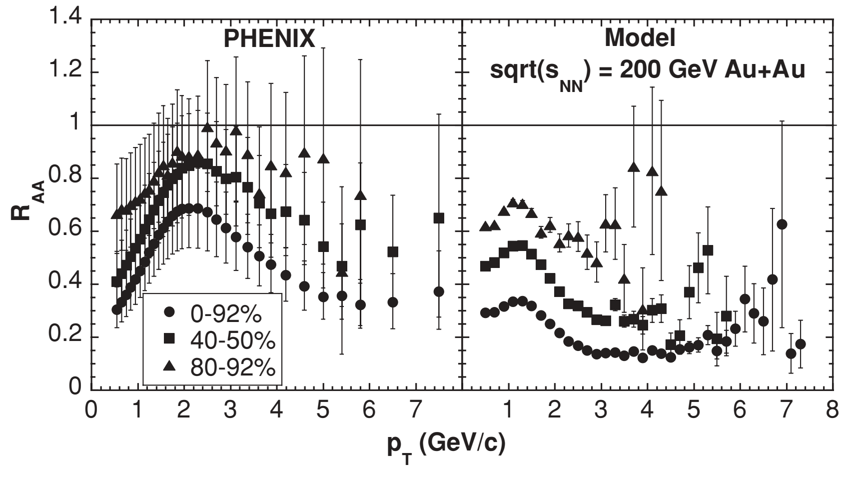

FIG. 16. R_{AA} for the model compared with PHENIX for several centralities.

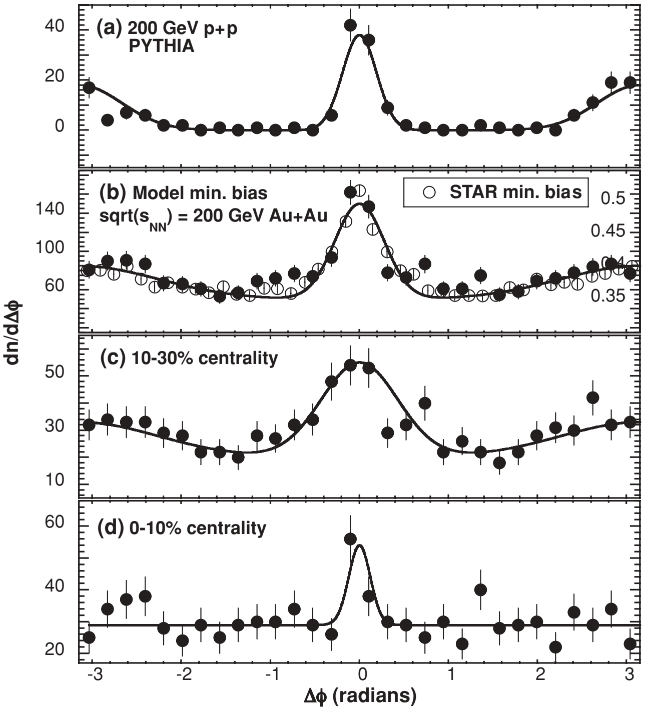

FIG. 17. $dn/d\Delta\phi$ vs $\Delta\phi$ plots using STAR cuts on p_T. (a) 200 GeV $p+p$ collisions from PYTHIA. (b) $\sqrt{s_{NN}} = 200$ GeV Au + Au with minimum bias centrality for the model and STAR. (c) $\sqrt{s_{NN}} = 200$ GeV Au + Au for the model with 10–30% centrality. (d) Same as (c) with 0–10% centrality. Fits to the points are also shown to guide the eye.

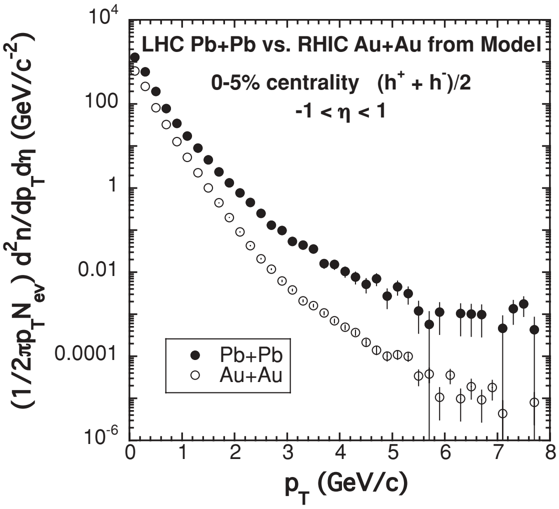

FIG. 19. p_T distributions from the model comparing LHC Pb + Pb and RHIC Au + Au collisions.

the model beyond $p+p$. As seen in Fig. 2, the rescattering rate is large in the early stage of the collision with some rescattering persisting to times of 50 fm/c and beyond. The radial flow effects seen in the identified particle m_T distributions of Fig. 5 and k_T dependence of the HBT parameters in Fig. 15 as well as the elliptic flow effects seen in the V_2 plots of Figs. 6–11 are mostly established in the early stage, i.e., by $t \approx$ 10 fm/c (see Fig. 18 of Ref. [18] for a calculation of $\sqrt{s_{NN}} =$ 200 GeV Au + Au collisions using a model similar to the present one). Comparison of the model with the experimental azimuthal HBT results shown in Figs. 13 and 14 provides a double test of the flow generated by the rescattering, since both radial flow effects, i.e., the sizes of the HBT parameters, and elliptic flow effects, i.e., their ϕ dependence, are present. While the present model gives a reasonably good description of the experimental elliptic flow results using rescattering effects alone, other cascade studies have found that either it is not possible to generate large enough elliptic flow [27,28] or it is necessary to use extreme elastic parton cross sections [29] to describe experiments. Although there are many differences in detail between the present study and those studies, the basic feature allowing the present model to generate enough elliptic

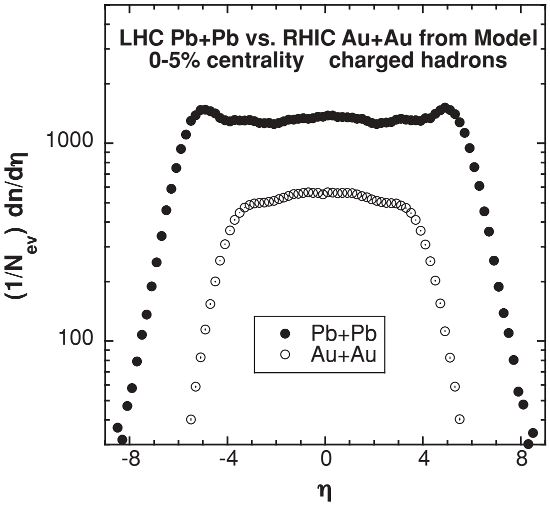

FIG. 18. Rapidity distributions from the model comparing Pb + Pb collisions at $\sqrt{s_{NN}} = 5.5$ TeV (LHC) with Au + Au collisions at $\sqrt{s_{NN}} = 200$ GeV (RHIC) for charged particles and 0–5% centrality.

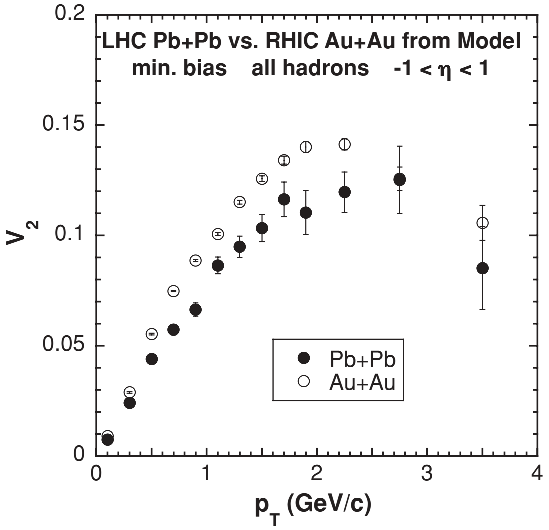

FIG. 20. V_2 vs p_T from the model comparing LHC Pb + Pb with RHIC Au + Au collisions; minimum bias centrality, all hadrons, and $-1 < \eta < 1$.

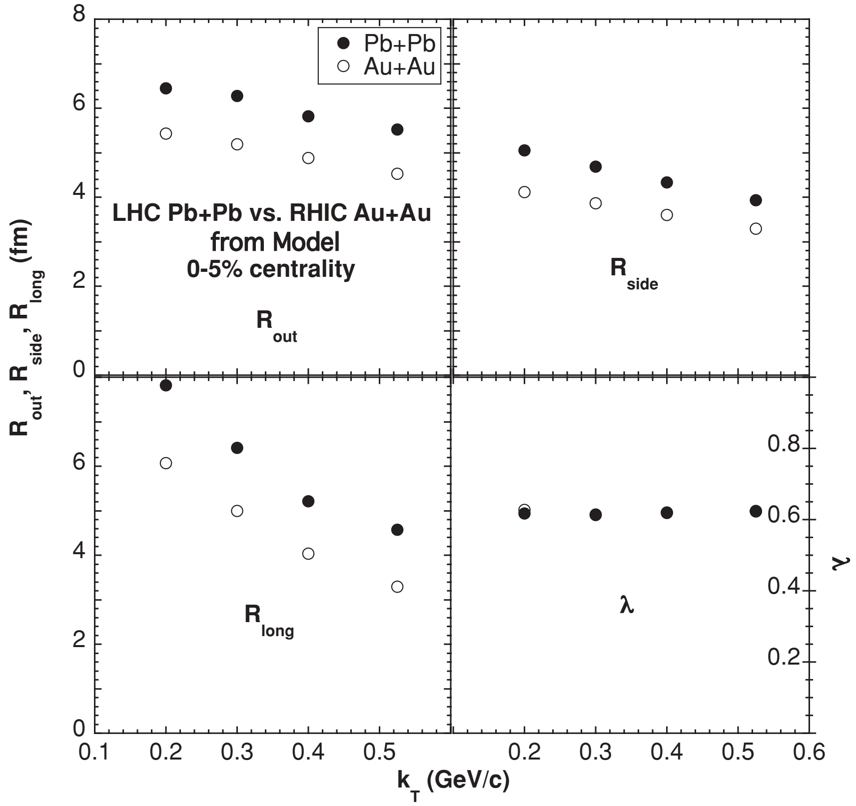

FIG. 21. Two-pion HBT vs k_T from the model comparing LHC Pb + Pb with RHIC Au + Au collisions; 0–5% centrality, $-0.5 < y < 0.5$, and $0.15 < p_T < 0.8$ GeV/c.

flow is that hadronic rescattering is allowed to take place from the earliest times and thus during the highest densities, as seen in Fig. 2. A concern regarding carrying out transport calculations at high densities is that nonphysical superluminal artifacts can be introduced which can affect the results [29]. As mentioned earlier, a study of this effect has been carried out for a model very similar to the present one, and it was found that the observables from the model studied, i.e., spectra, elliptic flow, and HBT, were not significantly affected [20]. Thus it is considered unlikely that these artifacts play a significant role in the present study.

This last statement should also be true for the $\sqrt{s_{NN}} =$ 5.5 TeV Pb + Pb predictions shown in Figs. 18–21. Although the rapidity density at midrapidity for LHC Pb + Pb is seen to be more than twice as large as for RHIC Au + Au in Fig. 18, the midrapidity particle density for LHC Pb + Pb for early times is found to be similar to that for RHIC Au + Au seen in Fig. 2. This is due to the larger hadronization volume and time resulting from the higher average particle momenta generated in the LHC-energy collisions, as seen in Fig. 19, and calculated from Eqs. (1)–(4). This similarity between the particle densities would explain why the flow effects seen in Figs. 20 and 21 are similar, i.e., the similarity between the LHC and RHIC elliptic flow and the dependence of the HBT radius parameters on k_T (although the overall size of the LHC radius parameters is greater).

The features of the high-p_T observables R_{AA} and $dn/d\Delta\phi$ calculated from the model and shown in Figs. 16 and 17 are also driven by the underlying rescattering. For these observables, it is the energy loss of the $p + p$ produced high-p_T particles rescattering with the rest of the particles that creates the effects. The effect of the rescattering can be seen for R_{AA} by considering that if the rescattering were turned off in the model, the numerator in Eq. (7), which would be simply a superposition of $p + p$ events, would be exactly the same distribution as the denominator except for a scale factor, resulting in a flat dependence on p_T for all centralities. The same would be the case for $dn/d\Delta\phi$ in Fig. 17 if rescattering were turned off: Fig. 17(d) would look like Fig. 17(a).

VI. SUMMARY AND CONCLUSIONS

A simple kinematic model based on superposition of $p + p$ collisions, relativistic geometry, and final-state hadronic rescattering has been used to calculate various hadronic observables in $\sqrt{s_{NN}} = 200$ GeV Au + Au collisions and $\sqrt{s_{NN}} = 5.5$ TeV Pb + Pb collisions. The model calculations were compared with experimental results from several $\sqrt{s_{NN}} = 200$ GeV Au + Au collision studies from RHIC. With the short hadronization time assumed in the model of $\tau = 0.1$ fm/c, it is found that this model describes the trends of the observables from these experiments surprisingly well considering the model's simplicity. This also gives more credibility to the model predictions presented for LHC-energy $\sqrt{s_{NN}} = 5.5$ TeV Pb + Pb collisions.

As shown above, the main strength of the present model is not that it gives precise agreement with experiment for individual observables in particular kinematic regions, but in its ability to give an overall qualitative description of a range of observables in a wide kinematic region, i.e., to summarize the gross features seen in experiments for $\sqrt{s_{NN}} = 200$ GeV Au + Au collisions. Another strength is its simplicity. Besides the kinematics generated in the superposed $p + p$ collisions by PYTHIA, the only other "active ingredient" in the model driving the kinematics underlying the hadronic observables shown is the final-state hadronic rescattering. As discussed above, if the hadronic rescattering were turned off in the model, all elliptic flow would disappear, the HBT radius parameters would lose all ϕ and k_T dependence and would be significantly smaller, the R_{AA} vs p_T plots would be flat, and all of the $dn/d\Delta\phi$ plots would look like $p + p$ [i.e., Fig. 17(a)]. Making τ large is another way to effectively turn off all of these effects, since the rescattering is very sensitive to this variable because it controls the initial particle density; e.g., for $\tau = 1$ fm/c, all these effects would already be greatly reduced [17].

The price to be paid for this simplicity is to assume that either hadrons or "hadron-like" objects can exist in the earliest stage of the heavy-ion collision just after the two nuclei pass through each other; i.e., that the hadronization time in the frame of the particle is short and insensitive to the environment in which it finds itself. Clearly this simple picture is an oversimplification as is seen in the model's shortcomings from the comparisons given above with RHIC experiments. However, some of these shortcomings could possibly be improved by "perturbatively" adding a few extra pieces of physics to this model, but thereby making it less simple.

ACKNOWLEDGMENTS

The author acknowledges enlightening discussions related to this work with Hans Bøggild, Ole Hansen, and Boris Tomasik; financial support from the US National Science Foundation under Grant PHY-0653432; and computing support from the Ohio Supercomputing Center.

---

[1] I. Arsene *et al.* (BRAHMS Collaboration), Nucl. Phys. **A757**, 1 (2005).
[2] B. B. Back *et al.* (PHOBOS Collaboration), Nucl. Phys. **A757**, 28 (2005).
[3] J. Adams *et al.* (STAR Collaboration), Nucl. Phys. **A757**, 102 (2005).
[4] K. Adcox *et al.* (PHENIX Collaboration), Nucl. Phys. **A757**, 184 (2005).
[5] B. B. Back *et al.* (PHOBOS Collaboration), Phys. Rev. Lett. **91**, 052303 (2003).
[6] J. Adams *et al.* (STAR Collaboration), Phys. Rev. Lett. **92**, 112301 (2004).
[7] S. S. Adler *et al.* (PHENIX Collaboration), Phys. Rev. C **69**, 034910 (2004).
[8] B. B. Back *et al.* (PHOBOS Collaboration), Phys. Rev. C **72**, 051901 (2005).
[9] J. Adams *et al.* (STAR Collaboration), Phys. Rev. C **72**, 014904 (2005).
[10] B. I. Abelev *et al.* (STAR Collaboration), Phys. Rev. C **77**, 054901 (2008).
[11] A. Adare *et al.* (PHENIX Collaboration), Phys. Rev. Lett. **98**, 162301 (2007).
[12] R. Hanbury Brown and R. Q. Twiss, Nature (London) **177**, 27 (1956).
[13] J. Adams *et al.* (STAR Collaboration), Phys. Rev. Lett. **93**, 012301 (2004).
[14] J. Adams *et al.* (STAR Collaboration), Phys. Rev. C **71**, 044906 (2005).
[15] C. Adler *et al.* (STAR Collaboration), Phys. Rev. Lett. **90**, 082302 (2003).
[16] T. Sjostrand, L. Lonnblad, S. Mrenna, and P. Skands, J. High Energy Phys. 05 (2006) 026.
[17] T. J. Humanic, Phys. Rev. C **76**, 025205 (2007).
[18] T. J. Humanic, Int. J. Mod. Phys. E **15**, 197 (2006).
[19] T. J. Humanic, Phys. Rev. C **57**, 866 (1998).
[20] T. J. Humanic, Phys. Rev. C **73**, 054902 (2006).
[21] T. Csorgo and J. Zimanyi, Nucl. Phys. **A517**, 588 (1990).
[22] M. Prakash, M. Prakash, R. Venugopalan, and G. Welke, Phys. Rep. **227**, 321 (1993).
[23] W. M. Yao *et al.* (Particle Data Group), J. Phys. G **33**, 1 (2006).
[24] T. J. Humanic, Phys. Rev. C **34**, 191 (1986).
[25] M. A. Lisa, S. Pratt, R. Soltz, and U. Wiedemann, Annu. Rev. Nucl. Part. Sci. **55**, 357 (2005).
[26] K. Aamodt *et al.* (ALICE Collaboration), J. Instrumentation, **3**, S08002 (2008).
[27] M. Bleicher *et al.*, J. Phys. G **25**, 1859 (1999).
[28] Q. Li, M. Bleicher, and H. Stocker, Phys. Lett. **B659**, 525 (2008).
[29] D. Molnar and M. Gyulassy, Nucl. Phys. **A697**, 495 (2002); [Erratum-*ibid.* **A703**, 893 (2002)].